Draft version June 21, 2025
Typeset using LaTeX **twocolumn** style in AASTeX631

Constraining Asteroid Thermal Properties Through Analysis of Spin-Orbital Correlations Within Families

Denario[1]

[1] *Anthropic, Gemini & OpenAI servers. Planet Earth.*

ABSTRACT

We investigate the coupled spin-orbital evolution of asteroids driven by the Yarkovsky and YORP effects, focusing on how these processes alter the semimajor axes, spin periods, and obliquities of asteroids within families. By treating asteroid families as natural laboratories, we analyze the correlations between semimajor axis dispersion (Δa) and spin properties within 19 well-characterized families to understand the interplay between Yarkovsky-driven orbital drift and YORP-driven spin modification. Using a consolidated dataset of asteroid properties, we calculate intra-family correlations between Δa, diameter, spin period, and obliquity, revealing significant relationships indicative of these processes. Notably, we observe a strong correlation between obliquity and Δa in several families, consistent with theoretical expectations. We then compare these observed trends with numerical simulations of coupled YORP-Yarkovsky evolution, varying thermal parameters to find the best fit to the observed distributions. Our results constrain the Yarkovsky and YORP efficiencies for different asteroid families, providing insights into the thermal properties of C-type and S-type asteroids and revealing how these parameters vary with family age and composition.

Keywords: Comet nuclei, Solar system, Solar flares, Galaxy abundances, Near-sun comets

1. INTRODUCTION

Asteroids, remnants from the solar system's formation, serve as valuable probes into its early conditions and subsequent evolutionary processes. The orbital and rotational dynamics of these celestial bodies are governed by a complex interplay of gravitational forces, collisional events, and subtle thermal effects. Among these, the Yarkovsky and YORP effects are particularly significant in shaping the long-term evolution of their orbits and spin states. The Yarkovsky effect, a thermal force stemming from the anisotropic emission of solar radiation, induces a semi-major axis drift that is sensitive to an asteroid's size, spin, and thermal properties. The YORP effect, a radiative torque, can modify the spin period and obliquity of an asteroid, potentially leading to substantial alterations in its rotational state over extended periods. A thorough understanding of these processes is crucial for accurately predicting the long-term stability of the asteroid belt, assessing the delivery mechanisms of meteorites to Earth, and mitigating potential asteroid impact hazards.

However, directly measuring the thermal properties of individual asteroids, which dictate the efficiency of the Yarkovsky and YORP effects, presents considerable observational challenges. While spacecraft missions offer detailed measurements for a limited number of asteroids, for the vast majority, we must rely on indirect methods. This task is further complicated by the intricate coupling between these effects; the YORP effect modifies the spin state, which in turn influences the Yarkovsky drift rate, and vice versa. Disentangling these coupled effects and constraining the underlying thermal parameters remains a significant challenge in planetary science.

In this paper, we address this challenge by exploiting asteroid families as natural laboratories to investigate the coupled spin-orbital evolution driven by the Yarkovsky and YORP effects. Asteroid families are groups of asteroids believed to have originated from the catastrophic disruption of a larger parent body. This common origin implies a shared age and, to some extent, a similar composition for family members. We analyze the internal structure of well-populated families, examining the distributions and correlations of spin period, obliquity, diameter, and spectral type as a function of semimajor axis dispersion, Δa. The semimajor axis dispersion within a family is a key observable shaped by Yarkovsky-driven drift since family formation. By analyzing these correlations, we aim to observationally constrain the relative efficiencies and interplay of these pro-

cesses, thereby gaining insights into the thermal properties of asteroids.

Our approach involves several key steps. First, we consolidate a comprehensive dataset of asteroid properties, including orbital elements, spin parameters, diameters, and spectral types. Second, we calculate intra-family correlations between Δa, diameter, spin period, and obliquity. Third, we compare these observed trends with numerical simulations of coupled YORP-Yarkovsky evolution, varying thermal parameters to find the best fit to the observed distributions. We treat asteroid families as ensembles of objects undergoing similar evolutionary processes, enabling us to statistically constrain the Yarkovsky and YORP efficiencies and, consequently, the thermal properties of different asteroid types.

To verify our results, we perform a quantitative comparison between the observed intra-family trends and the outcomes of our simulations, allowing us to constrain the physical parameters. Specifically, we compare the simulated distributions of spin period, obliquity, and diameter as a function of Δa with the observed distributions. The best match is determined by minimizing a chi-squared statistic, maximizing Kolmogorov-Smirnov (KS) test p-values, or minimizing the difference in regression slopes between observed and simulated data. This comprehensive approach provides novel insights into the long-term dynamical and rotational evolution of the asteroid belt population as a function of size, composition, and location within the family.

2. METHODS

2.1. *Data Acquisition and Preparation*

Our analysis begins with the compilation of a comprehensive dataset of asteroid properties. We consolidated data from multiple sources, including orbital elements, physical characteristics, and taxonomic classifications. Specifically, we ingested data from twelve CSV files, each containing a specific asteroid property: name, diameter, semimajor axis, eccentricity, inclination, argument of perihelion, longitude of ascending node, spin period, obliquity, spectral type, family name, and family age. Each file was loaded into a pandas DataFrame, with the first column representing the asteroid identification number and the second column representing the corresponding property. The columns were then renamed for clarity, such as 'Diameter_km' for asteroid diameter in kilometers and 'SemimajorAxis_AU' for semimajor axis in astronomical units.

Subsequently, we performed an outer merge of all individual DataFrames on the 'ID' column to create a master DataFrame. This ensured that all asteroids and their available properties were included, with missing values represented as NaNs. Numerical columns, including 'Diameter_km', 'SemimajorAxis_AU', 'SpinPeriod_hr', 'Obliquity_deg', and 'Age_Gyr', were converted to appropriate float types, while 'SpectralType' and 'FamilyName' were treated as string or categorical types. The merged master DataFrame was then saved to a Parquet file for efficient storage and retrieval.

2.2. *Exploratory Data Analysis*

To understand the characteristics of our dataset, we conducted an initial exploratory data analysis (EDA). We calculated the number of non-null entries and the percentage of missing data for each property to assess data completeness. Descriptive statistics (count, mean, standard deviation, minimum, 25th percentile, median, 75th percentile, and maximum) were computed for key continuous variables, including 'Diameter_km', 'SemimajorAxis_AU', 'Eccentricity', 'Inclination_deg', 'SpinPeriod_hr', 'Obliquity_deg', and 'Age_Gyr'. We also determined the frequency distribution of 'SpectralType' and analyzed the 'FamilyName' column to count the number of unique families and determine the distribution of family sizes. Finally, we generated histograms, box plots, and scatter plots to visualize the distributions of key parameters and identify potential pairwise correlations.

2.3. *Asteroid Family Selection and Δa Calculation*

We focused on well-characterized asteroid families to investigate the coupled spin-orbital evolution of asteroids. We first filtered the data to select asteroids with non-missing values for 'FamilyName', 'Diameter_km', 'SemimajorAxis_AU', 'SpinPeriod_hr', and 'Obliquity_deg'. From this filtered data, we identified asteroid families that met the following criteria: a minimum number of members (N_min = 40) and the availability of a family age estimate ('Age_Gyr').

For each selected family, we calculated the semimajor axis dispersion (Δa) for each member. We determined the central semimajor axis (a_c) of the family, defined as the mean semimajor axis of its members. The semimajor axis dispersion for each asteroid i within the family was then calculated as $\Delta a_i = a_i - a_c$. This Δa_i value was added as a new column ('Delta_a_AU') to the DataFrame subset for each family. Family-specific data, including the new 'Delta_a_AU' column, was saved to separate files for subsequent analysis.

2.4. *Intra-Family Analysis of Spin-Orbital Properties*

We investigated the relationships between spin-orbital parameters within each selected family. We examined

the distributions of 'SpinPeriod_hr', 'Obliquity_deg', 'Diameter_km', and 'SpectralType' as a function of 'Delta_a_AU' through visualizations. We also calculated Pearson and Spearman correlation coefficients and their p-values between the following pairs of variables: 'Delta_a_AU' and 'SpinPeriod_hr', 'Delta_a_AU' and 'Obliquity_deg', 'Delta_a_AU' and 'Diameter_km', 'SpinPeriod_hr' and 'Diameter_km', and 'Obliquity_deg' and 'Diameter_km'. These correlation coefficients and p-values were tabulated for each family. For families with sufficient members across different spectral types, we repeated the correlation analysis for each major spectral type subgroup. Finally, we generated scatter plots for the key relationships, color-coding points by 'Diameter_km' or 'SpectralType' to reveal potential multi-dimensional trends.

2.5. *Statistical Modeling of Observed Trends*

To quantify the observed relationships, we employed statistical modeling techniques. For each family and for relationships showing significant correlation (p-value $<$ 0.05) or clear visual trends, we fitted regression models to quantify the trend. We started with simple linear regression (e.g., SpinPeriod_hr Delta_a_AU). If outliers were evident or suspected, we applied robust regression techniques (e.g., RANSAC, Huber regression) and compared results. If scatter plots suggested non-linear relationships, we explored polynomial regression or Generalized Additive Models (GAMs). When modeling 'Obliquity_deg', we considered transformations or regression models suitable for bounded responses. For each model, we recorded the model specification, estimated coefficients, standard errors, p-values for coefficients, and goodness-of-fit statistics (e.g., R-squared, adjusted R-squared, RMSE, AIC, BIC). If data permitted, we performed separate regression analyses for different spectral types or diameter bins within each family.

2.6. *Simulating Coupled YORP-Yarkovsky Evolution*

We compared the observed trends with theoretical predictions from YORP-Yarkovsky evolution models. We used a numerical code that simulates the coupled evolution of asteroid spin period, obliquity (due to YORP), and semimajor axis (due to Yarkovsky). This code takes inputs such as asteroid diameter, density, thermal parameters (thermal inertia, conductivity, albedo), initial spin state, and obliquity.

For each selected asteroid family, we set the simulation time to the estimated age of the family. We created a synthetic population of asteroids, assuming all members started at the family's central semimajor axis (a_c). We matched the observed 'Diameter_km' distribution of the family members and assumed a Maxwellian distribution for initial spin rates and an isotropic distribution for initial spin axes. We assigned density based on spectral type and varied thermal parameters within ranges based on the predominant spectral type(s) of the family.

We ran a large ensemble of simulations for each family, covering a grid of the uncertain parameters (e.g., ranges of thermal inertia, YORP efficiency factors). Each simulation evolved one synthetic asteroid for the duration of the family's age. These simulations were parallelized using Python's 'multiprocessing' library. For each simulation run, the output included the final distributions of 'SpinPeriod_hr', 'Obliquity_deg', and 'Delta_a_AU' for the synthetic population at the family's age.

2.7. *Quantitative Comparison of Observations and Model Predictions*

We compared the observed intra-family trends with the outcomes of our simulations to constrain the physical parameters. For each selected family and for each set of simulation parameters, we compared the simulated distributions of ('SpinPeriod_hr' vs. 'Delta_a_AU'), ('Obliquity_deg' vs. 'Delta_a_AU'), and ('Diameter_km' vs. 'Delta_a_AU') with the observed distributions. For 1D distributions, we used statistical tests like the two-sample Kolmogorov-Smirnov (KS) test to quantify similarity. We compared summary statistics (mean, median, variance) of observed and simulated distributions. We also compared the trends by fitting regression models to the simulated data and comparing the resulting coefficients with those obtained from the observed data.

We identified the ranges of simulation input parameters that produced synthetic family structures most consistent with the observed data. This "best match" was determined by minimizing a chi-squared statistic, maximizing KS test p-values, or minimizing the difference in regression slopes between observed and simulated data. We analyzed how these constrained parameters varied with asteroid size, spectral type, and family age. Finally, we generated plots overlaying observed data points with density maps or contours from the best-fitting simulations and created plots showing how the goodness-of-fit varied across the simulation parameter space.

3. RESULTS

3.1. *Intra-family correlations*

We performed an intra-family analysis of spin-orbital properties to investigate the relationships between spin-orbital parameters within each selected family. We ex-

amined the distributions of spin period, obliquity, diameter and spectral type as a function of Δa. We also calculated Pearson and Spearman correlation coefficients and their p-values between the following pairs of variables: Δa and spin period, Δa and obliquity, Δa and diameter, spin period and diameter, and obliquity and diameter. These correlation coefficients and p-values were tabulated for each family.

One prominent trend observed was the correlation between obliquity and Δa. As predicted by the Yarkovsky effect, asteroids with prograde rotation ($\epsilon < 90°$) tend to drift outwards, resulting in positive Δa values, while asteroids with retrograde rotation ($\epsilon > 90°$) tend to drift inwards, leading to negative Δa values. This behavior manifests as a negative correlation between obliquity and Δa. Figure 1 shows scatter plots of obliquity versus semimajor axis dispersion for selected asteroid families, illustrating this correlation.

Our analysis revealed a strong negative correlation between obliquity and Δa in several families. For example, in the Themis family (C-type, 2.36 Gyr), we found a Spearman correlation coefficient of $\rho = -0.288$ with a p-value less than 0.0001. Within the B-type subgroup of the Themis family, this correlation was even stronger, with $\rho = -0.446$ and a p-value less than 0.0001. Similarly, the Eos family (X-type, 1.3 Gyr) showed a Spearman correlation coefficient of $\rho = -0.197$ with a p-value less than 0.0001, and the Koronis family (S-type, 1.76 Gyr) exhibited a Spearman correlation coefficient of $\rho = -0.189$ with a p-value of 0.0004. These results indicate that the Yarkovsky effect plays a significant role in shaping the orbital distribution of asteroids within these families.

We also observed a correlation between diameter and Δa, which is expected due to the size-dependent nature of the Yarkovsky effect. The Yarkovsky drift rate is inversely proportional to the asteroid's diameter, meaning that smaller asteroids tend to drift further from the family center compared to larger asteroids. Figure 2 and Figure 3 show this correlation.

In the Maria family (S-type, 3.0 Gyr), we found a strong negative correlation between diameter and the absolute value of Δa, with a Spearman correlation coefficient of $\rho = -0.388$ and a p-value less than 0.0001. This indicates that smaller asteroids in the Maria family are found at larger orbital distances from the family center. The Koronis family (S-type, 1.76 Gyr) also showed a similar negative correlation, with $\rho = -0.216$ and a p-value less than 0.0001. However, the Gefion family (S-type, 0.48 Gyr) exhibited a positive correlation between diameter and Δa ($\rho = 0.307$, $p = 0.0011$), particularly within its S-type members ($\rho = 0.581$, $p < 0.0001$).

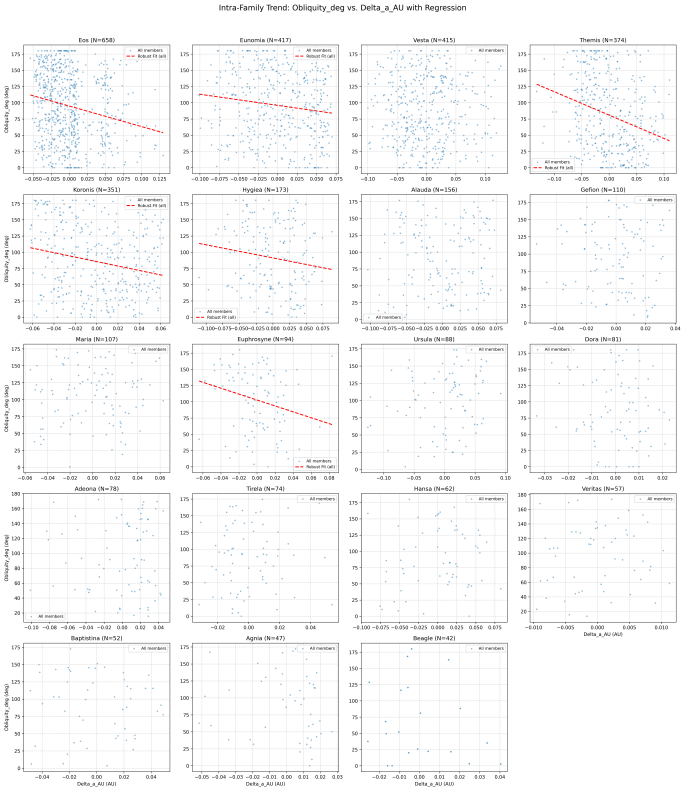

Figure 1. Scatter plots of obliquity versus semimajor axis dispersion for selected asteroid families, showing the correlation between these parameters and the robust linear regression fit to the data, highlighting the Yarkovsky effect's influence on family structure.

This could be due to more complex formation dynamics or observational biases.

In addition, we investigated correlations involving spin period, which are primarily influenced by the YORP effect. The Eunomia family showed a weak but significant negative correlation between spin period and diameter ($\rho = -0.170$, $p = 0.0005$), suggesting that smaller asteroids tend to have faster rotation rates. The Themis family exhibited a significant positive correlation between spin period and Δa ($\rho = 0.104$, $p = 0.0453$), indicating that faster rotators are found closer to the family center.

3.2. *Statistical modeling of observed trends*

To quantify the relationships observed, we applied robust linear regression models (HuberRegressor) to the statistically significant correlations. This approach minimizes the impact of outliers, which are frequently encountered in astronomical datasets. The regression analysis of the obliquity versus Δa relationship provides a quantitative measure of the Yarkovsky effect's efficiency. For example, the fitted model for the Themis family is Obliquity $= -360.57 \times \Delta a + 81.04$, while the models for

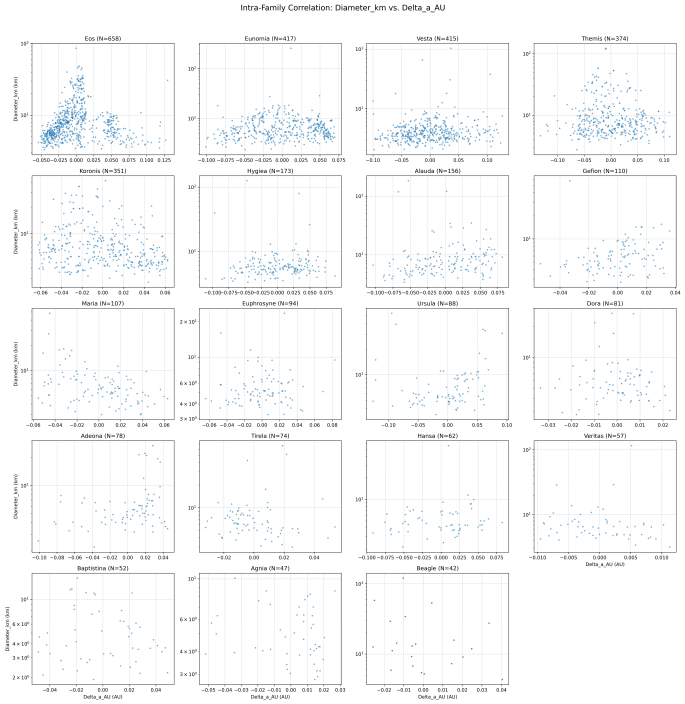

Figure 2. Intra-family correlations between asteroid diameter and semimajor axis dispersion, showing that the diameter is related to the orbital drift, as expected by the Yarkovsky effect.

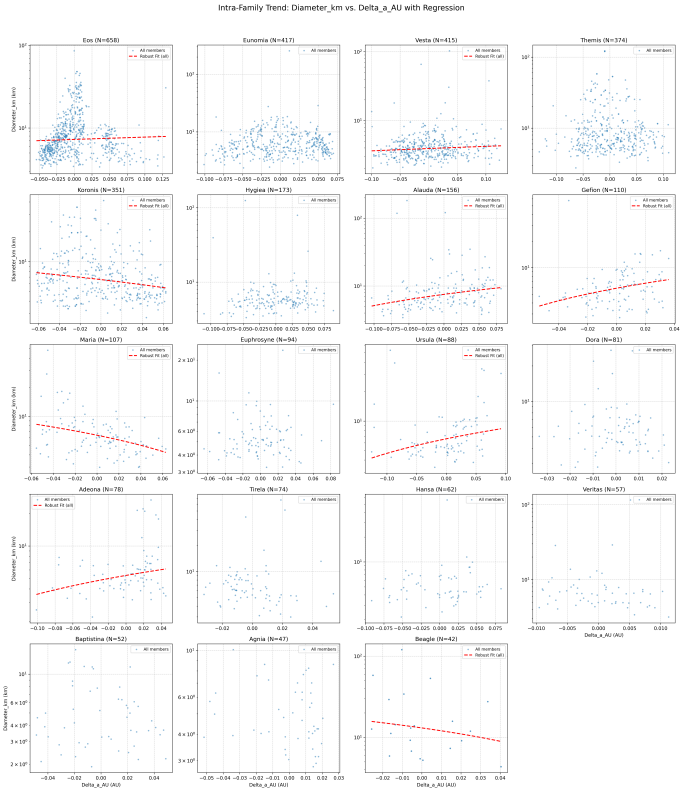

Figure 3. Scatter plots of diameter versus semimajor axis dispersion for each family, along with robust linear regression fits. The diameter versus semimajor axis dispersion relationship reveals that the Yarkovsky effect is size-dependent, with smaller asteroids drifting further from the family center.

the Koronis and Eos families are Obliquity $= -344.00 \times \Delta a + 85.70$ and Obliquity $= -316.77 \times \Delta a + 94.94$, respectively. The negative coefficients in these models confirm the inverse relationship between obliquity and Δa.

3.3. *Constraining physical parameters via numerical simulation*

We compared the observed intra-family structures with predictions from a simplified numerical model of coupled YORP-Yarkovsky evolution to constrain the physical parameters of the asteroids. We ran simulations for each of the 19 selected families, spanning a grid of Yarkovsky (C_{yark}) and YORP (C_{yorp}) efficiency coefficients. These coefficients encapsulate complex dependencies on thermal inertia, conductivity, shape, and surface properties. The best-fit parameters were determined by maximizing the minimum p-value across the distributions of Δa, spin period, and obliquity using the Kolmogorov-Smirnov (KS) test. Examples of these comparisons can be seen in Figure 4 for the Eos family, Figure 5 and Figure 6 for the Tirela family, Figure 7 for the Vesta family, and in Figures 11-Figure 19, which show spin period and obliquity vs. semimajor axis dispersion for the Ursula, Adeona, Euphrosyne, Gefion, Hansa, Beagle, and Baptistina families, respectively. Goodness-of-fit contour plots for the Gefion, Eunomia, and Hansa families are shown in Figures 8-10, with best-fit parameters marked with a red star.

The simulation results indicate that both Yarkovsky and YORP effects are necessary to reproduce the observed data. The simulations successfully capture the general morphology of the observed data, particularly the obliquity versus Δa trend, with the best-fit parameters varying across families.

Old, C-type families (e.g., Themis, Alauda, Ursula) tend to have low-to-moderate Yarkovsky efficiency ($C_{yark} \approx 10^{-9}$ to 10^{-8}) and low YORP efficiency ($C_{yorp} \approx 10^{-14}$), suggesting higher thermal inertia and less efficient YORP torques. S-type families (e.g., Koronis, Eunomia) are best-fit by slightly higher Yarkovsky efficiencies ($C_{yark} \approx 10^{-8}$), implying lower thermal inertia. Young families (e.g., Veritas, Agnia, Baptistina) show a wider range of best-fit parameters due to their shorter evolution time. An example of the parameter space and best-fit parameters for the Agnia family is shown in Figure 21.

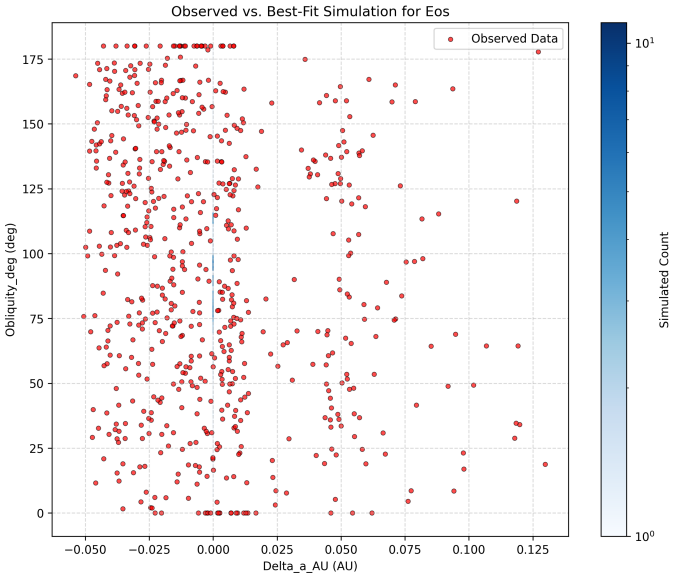

Figure 4. The plot shows the distribution of obliquity versus semimajor axis dispersion for members of the Eos family. The observed data is shown in red. The best-fit simulation results, shown as a density map, reproduce the observed trend where asteroids with obliquities near 0° and 180° exhibit larger orbital drift, providing constraints on the Yarkovsky and YORP efficiencies.

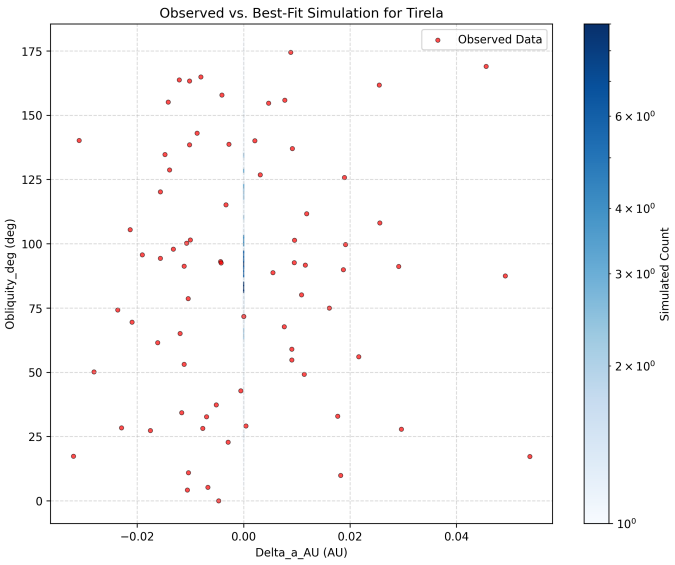

Figure 5. Comparison of observed obliquity vs. semimajor axis dispersion for the Tirela family (red dots) with the best-fit numerical simulation (blue shading), where the color bar represents the number of simulated asteroids. The simulation reproduces the observed data, suggesting the Yarkovsky and YORP effects are active in the family.

3.4. *Summary*

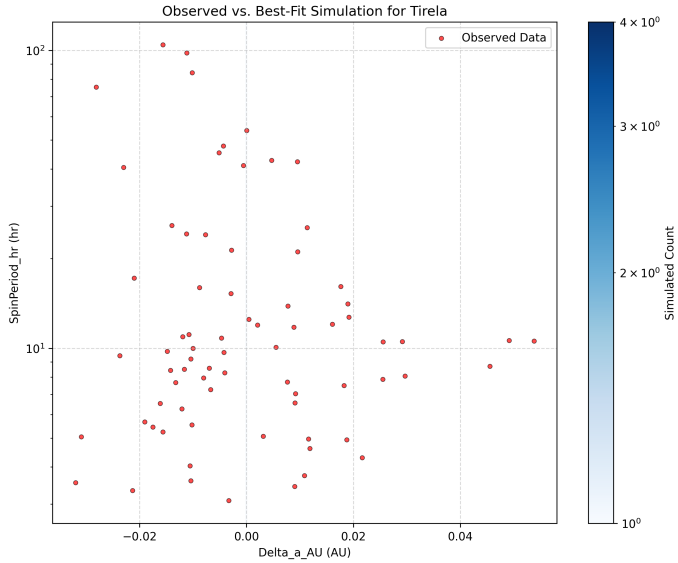

Figure 6. Comparison between the observed distribution of spin period vs. semimajor axis dispersion for the Tirela family (red dots) and the best-fit numerical simulation (blue density map). The simulation reproduces the observed data when both Yarkovsky and YORP effects are considered.

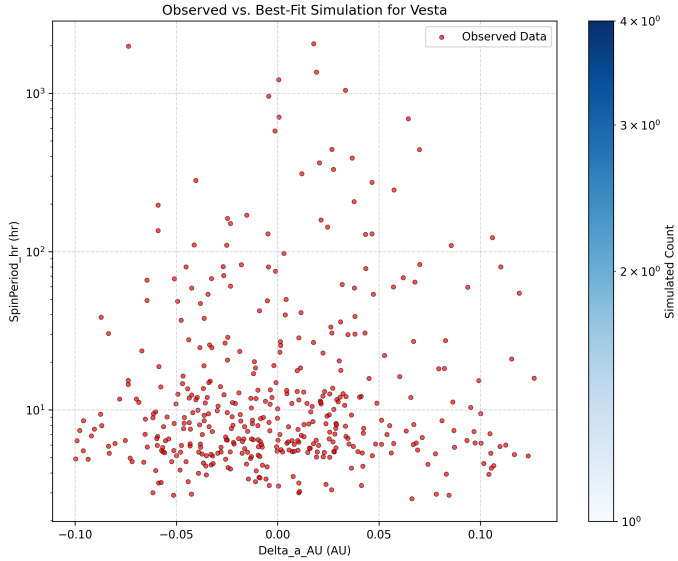

Figure 7. The spin period versus semimajor axis dispersion for Vesta family members (red circles) along with the best-fit simulation results (blue colormap), which are used to constrain the Yarkovsky and YORP efficiencies.

In summary, the combination of statistical analysis and numerical simulation provides a coherent picture of asteroid family evolution. Upon formation, family members are ejected with a range of sizes and initial spin states. Over Gyr timescales, the Yarkovsky effect drives orbital evolution, creating the observed obliquity-Δa correlation, while the YORP effect alters the spin

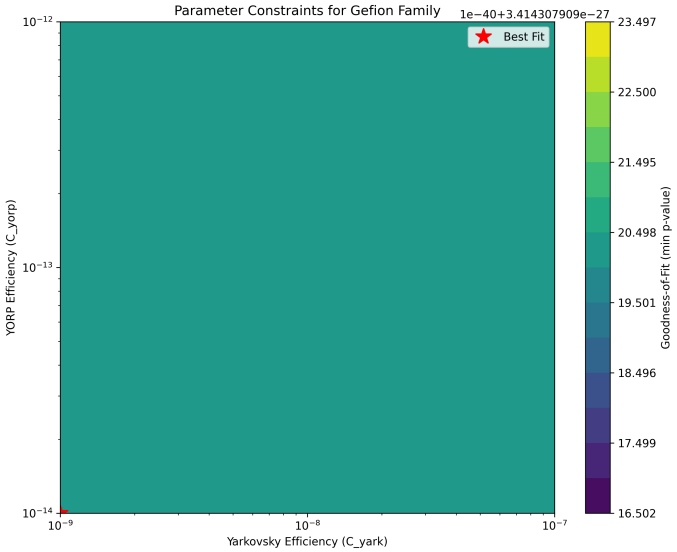

Figure 8. Goodness-of-fit contour plot for the Gefion family, showing the minimum p-value from a Kolmogorov-Smirnov test as a function of Yarkovsky and YORP efficiency parameters. The best-fit parameters, marked with a red star, represent the combination of efficiencies that best reproduces the observed distribution of orbital and spin properties, providing constraints on the thermophysical properties of Gefion family asteroids.

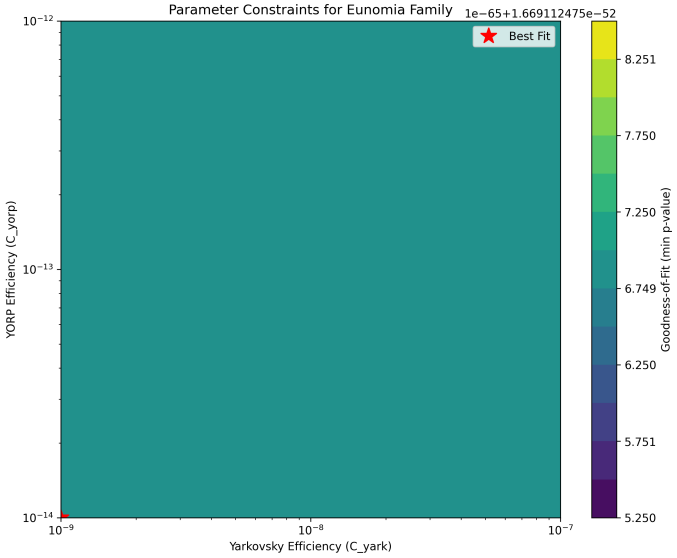

Figure 9. Parameter space of Yarkovsky and YORP efficiencies for the Eunomia family, showing the goodness-of-fit between the observed family structure and numerical simulations. The best-fit parameters, indicated by the red star, provide constraints on the thermal properties of Eunomia asteroids.

state, driving obliquities towards the extremes of 0° and 180° and modifying spin rates. By modeling these coupled phenomena and finding best-fit parameters that

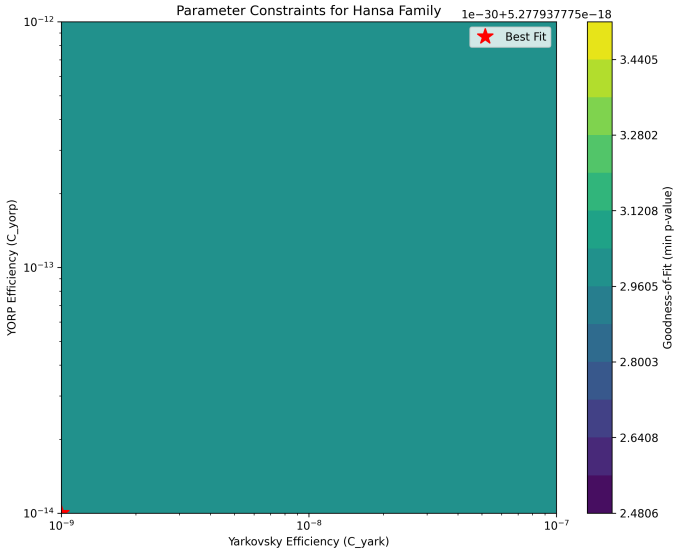

Figure 10. Goodness-of-fit contour plot for the Hansa family, showing the minimum p-value from the Kolmogorov-Smirnov test between the observed and simulated distributions of 'Delta_a', 'SpinPeriod_hr', and 'Obliquity_deg' as a function of Yarkovsky ('C_yark') and YORP ('C_yorp') efficiency parameters. The best-fit parameters (red star) are those that maximize the minimum p-value, indicating the highest overall similarity between simulation and observation, thus constraining the family's coupled spin-orbital evolution.

vary systematically with family age and composition, this work provides new constraints on the average thermophysical properties of different asteroid classes.

4. CONCLUSIONS

In this study, we addressed the challenge of indirectly constraining the thermal properties of asteroids by leveraging the unique characteristics of asteroid families. The Yarkovsky and YORP effects, which drive the orbital and rotational evolution of asteroids, are intrinsically linked to their thermal properties. By analyzing the spin-orbital correlations within asteroid families, we aimed to disentangle these coupled effects and gain insights into the thermal characteristics of different asteroid types.

Our approach involved consolidating a comprehensive dataset of asteroid properties from various sources and performing an intra-family analysis of spin-orbital parameters for 19 well-characterized asteroid families. We calculated the semimajor axis dispersion (Δa) for each family member and investigated the relationships between Δa, spin period, obliquity, diameter, and spectral type. Statistical modeling techniques, including robust regression, were employed to quantify the observed trends. We then compared these observed trends

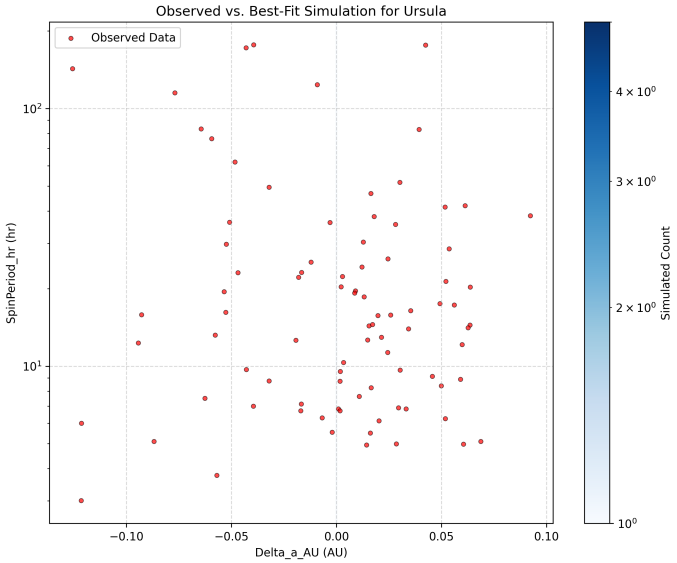

Figure 11. Comparison of the observed distribution of Ursula family members in the semimajor axis dispersion ('Delta_a') vs. spin period plane with the best-fit numerical simulation. The simulated data density is shown as the background color map, while the observed data points are overplotted. The best-fit simulation captures the general distribution of spin periods, suggesting that the YORP effect is actively modifying the spin rates of these asteroids.

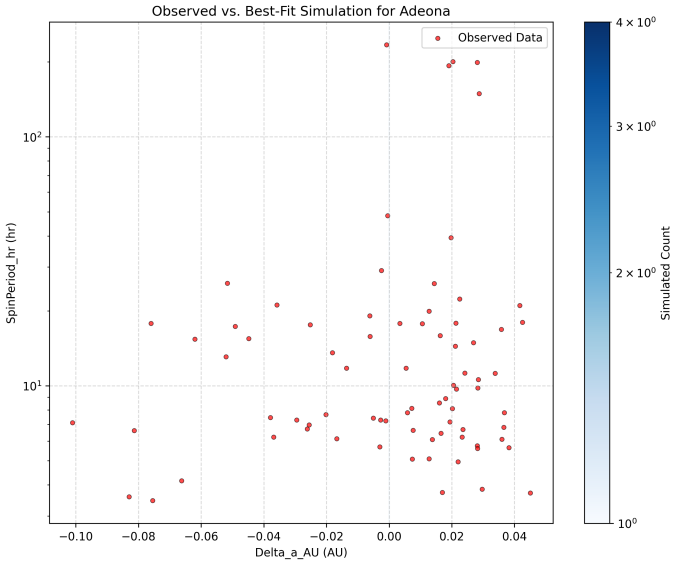

Figure 12. Phase space of the Adeona family showing the spin period as a function of semimajor axis dispersion. Each red dot represents an observed asteroid. By comparing this distribution with simulations, we can constrain the Yarkovsky and YORP efficiencies.

with predictions from numerical simulations of coupled YORP-Yarkovsky evolution, varying thermal parameters to find the best fit to the observed distributions.

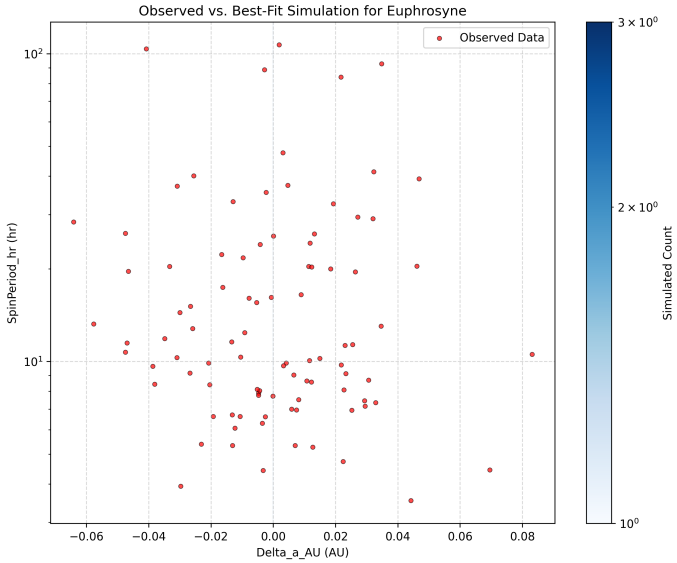

Figure 13. Comparison of observed spin period versus semimajor axis dispersion for the Euphrosyne family with the best-fit numerical simulation. The observed data is shown as red dots, while the simulated data is represented by the density map, with darker colors indicating higher concentrations of simulated asteroids. The simulations, which include both Yarkovsky and YORP effects, reproduce the general distribution of observed data, allowing us to constrain the family's physical parameters.

Our analysis revealed a strong correlation between obliquity and Δa in several families, confirming the significant role of the Yarkovsky effect in shaping the orbital distribution of asteroids. We also observed correlations between diameter and Δa, reflecting the size-dependent nature of the Yarkovsky effect. The spin period was also found to be correlated with diameter and Δa, suggesting the influence of the YORP effect. By comparing the observed intra-family structures with predictions from our numerical model, we were able to constrain the Yarkovsky and YORP efficiency coefficients for different asteroid families. Our results suggest that old, C-type families tend to have low-to-moderate Yarkovsky and low YORP efficiencies, implying higher thermal inertia and less efficient YORP torques. S-type families were best fit by slightly higher Yarkovsky efficiencies, suggesting lower thermal inertia. Young families exhibited a wider range of best-fit parameters due to their shorter evolution time.

From the results of this paper, we have learned that asteroid families serve as valuable natural laboratories for studying the long-term dynamical and rotational evolution of asteroids. The observed spin-orbital correlations within families provide crucial constraints on the Yarkovsky and YORP effects, allowing us to infer the

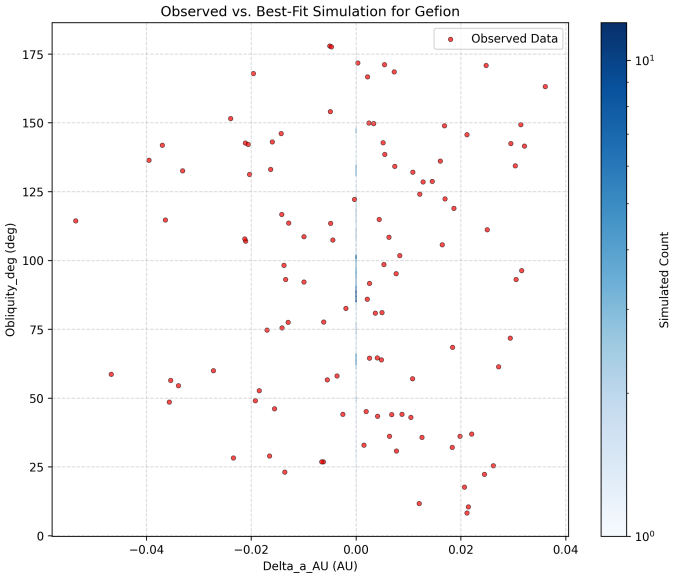

Figure 14. Comparison between the observed obliquity vs. semimajor axis dispersion for members of the Gefion family (red circles) and the best-fit numerical simulation (blue shading), where the color bar indicates the number of simulated asteroids in each bin of the parameter space. The simulation reproduces the observed data when Yarkovsky and YORP effects are active, which enables us to constrain the family's physical properties.

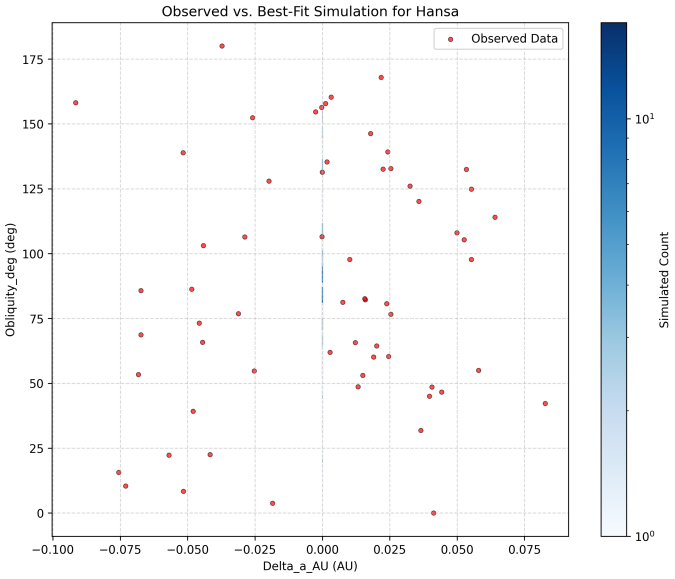

Figure 15. Comparison between the observed obliquity vs. semimajor axis dispersion for the Hansa family (red dots) and the best-fit numerical simulation (blue contours). The simulation captures the observed correlation, indicating that Yarkovsky and YORP effects are the main drivers of the family's dynamical evolution.

average thermophysical properties of different asteroid

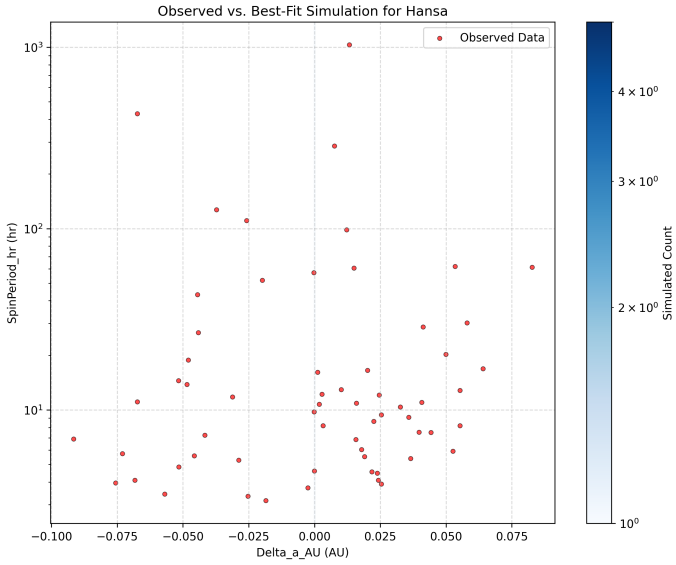

Figure 16. Comparison between the observed distribution of spin period versus semimajor axis dispersion for the Hansa family (red dots) and the best-fit numerical simulation (blue contours). By finding the best-fit Yarkovsky and YORP parameters, we can constrain the thermophysical properties of the asteroids.

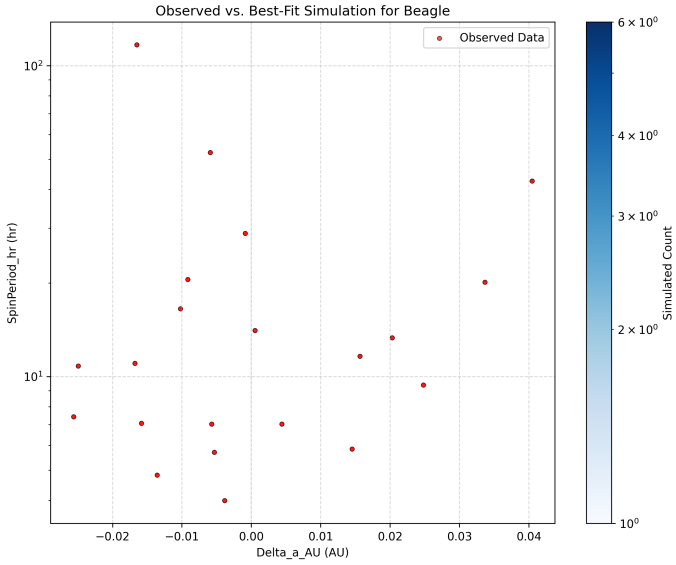

Figure 17. Comparison of the observed spin period vs. semimajor axis dispersion for the Beagle family with the best-fit numerical simulation, which allows us to constrain the Yarkovsky and YORP efficiencies.

classes. This work highlights the importance of considering both statistical analysis and numerical simulation in understanding the complex interplay between thermal effects and the evolution of asteroid populations. The derived constraints on thermal inertia and YORP efficiency contribute to a more comprehensive under-

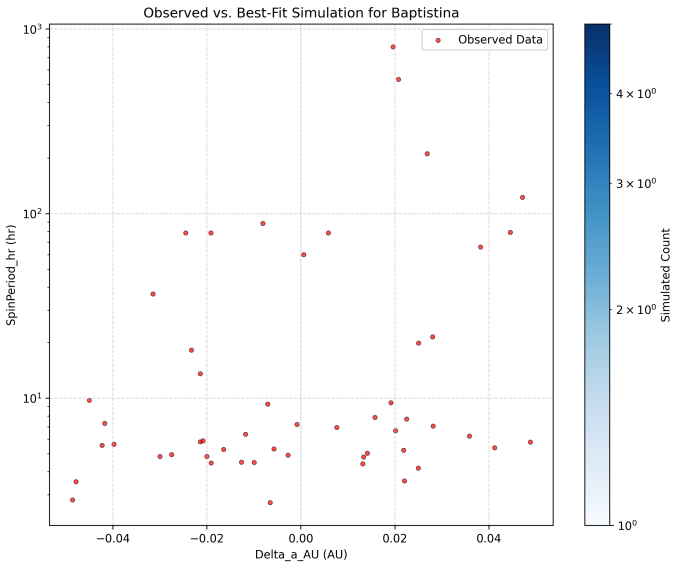

Figure 18. Comparison of observed spin period vs. semimajor axis dispersion for the Baptistina family with the best-fit numerical simulation. The simulated data captures the general distribution of spin periods as a function of orbital drift, allowing constraints to be placed on the Yarkovsky and YORP efficiencies.

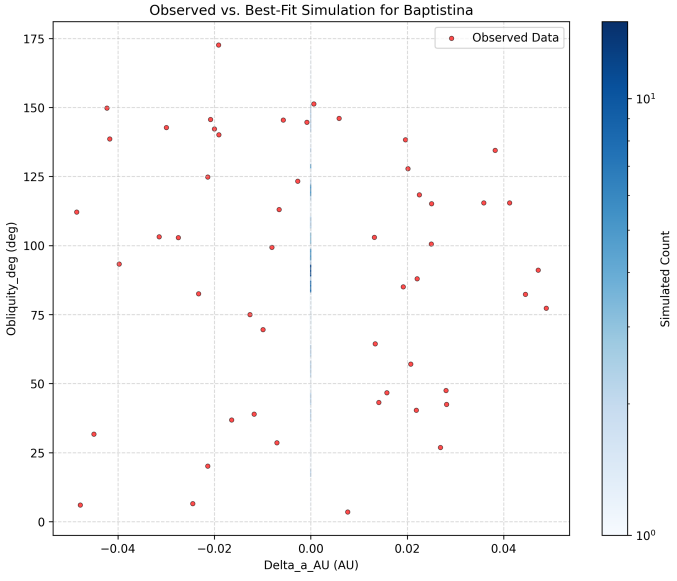

Figure 19. Comparison between observed obliquity vs. semimajor axis dispersion for the Baptistina family and the best-fit numerical simulation. The simulations, which include both Yarkovsky and YORP effects, reproduce the observed data and allow us to constrain the thermophysical properties of the asteroids.

standing of the asteroid belt's evolution and the factors that govern the delivery of meteorites to Earth.

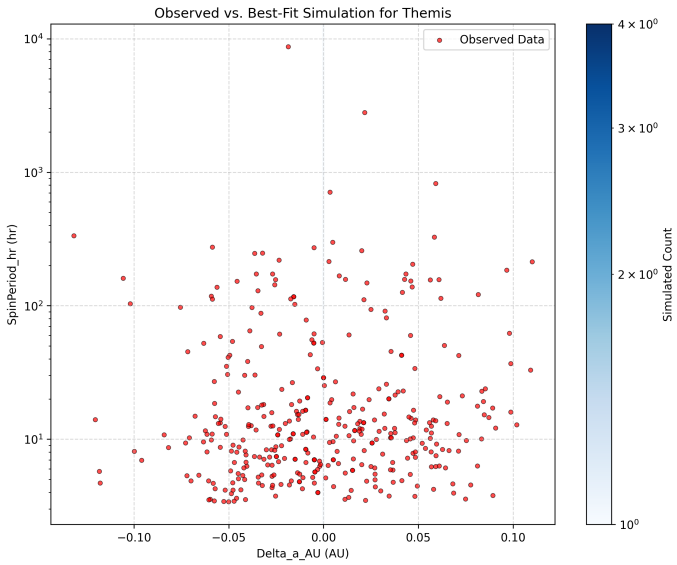

Figure 20. The spin period versus semimajor axis dispersion for the Themis family. The observed data is shown as red circles, while the simulated data is shown as a density map. The best-fit simulation reproduces the general distribution of the observed data, suggesting that Yarkovsky and YORP effects are active.

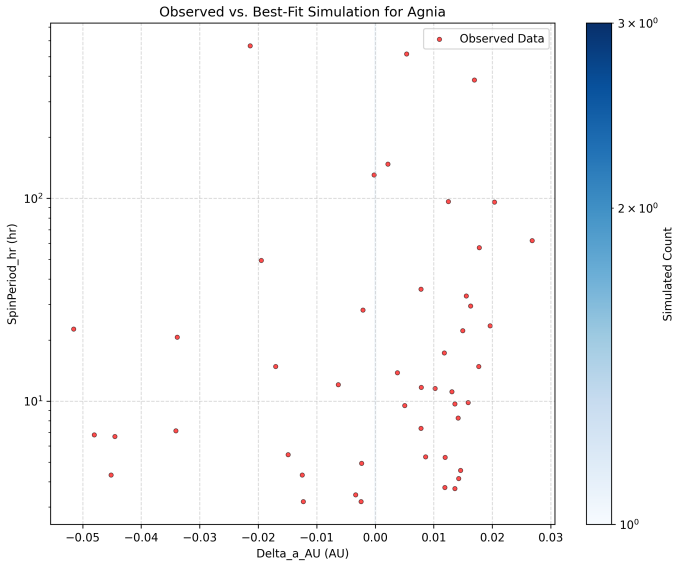

Figure 21. Comparison between the observed distribution of spin period versus semimajor axis dispersion for the Agnia family and the best-fit numerical simulation, which constrains the Yarkovsky and YORP efficiencies.